Fast-response dual-beam UV-absorption ozone photometer suitable for use on stratospheric balloons

Michael H. Proffitt

Aeronomy Laboratory, National Oceanic and Atmospheric Administration, Environmental Research Laboratories, Boulder, Colorado 80303 and Cooperative Institute for Research in Environmental Sciences, University of Colorado/National Oceanic and Atmospheric Administration, Boulder, Colorado 80309

Richard J. McLaughlin

Aeronomy Laboratory, National Oceanic and Atmospheric Administration, Environmental Research Laboratories, Boulder, Colorado 80303

(Received 2 June 1983; accepted for publication 30 August 1983)

Various types of ozone detectors are currently in use, each with different advantages and compromises in response time, portability, sensitivity, accuracy, need for repeated calibration, and expense. We describe here a new dual-beam UV-absorption instrument for balloon-borne measurements of atmospheric ozone. It has two identical absorption chambers, each alternating between reference mode (ozone free) and sample mode by means of a four-port valve and ozone scrubber. The ratio of the absorption signals, along with the known lengths and ozone absorption cross section, yield the ozone concentration. The dual-beam feature cancels the effects of lamp intensity fluctuations, while the mode alternation compensates for mechanical changes and also provides continuous measurements. The absorption measurement requires no calibration and, hence, is independent of gas flow rate. The response time is 1 s and, for this measurement duration, the minimum ozone concentration detectable by this instrument (one standard deviation) is 1.5×10^{10} molecules/cm^3 (0.6 ppbv at STP). The overall uncertainty of a 1-s measurement at the ozone maximum (22 km) is 3.6%, where 2% of this is the accuracy of the ozone cross section. The size and weight are suitable for launch by small balloons, but the cost of the instrument precludes its use as a disposable unit.

PACS numbers: 07.60.Dq, 94.10.Fa, 93.85. + q, 82.80.Di

INTRODUCTION

Although occurring only in trace amounts, the presence of ozone in the atmosphere is crucially important to our quality of life. The absorption of solar ultraviolet radiation by *stratospheric* ozone (12 to 50 km) protects the biosphere from harmful radiation. Furthermore, the absorption of surface infrared radiation by *tropospheric* ozone (surface to 12 km) is a factor in the global temperature balance. Lastly, the photochemical reactivity of ozone influences the chemical composition of both the stratosphere and the troposphere. Thus, to a rather major extent, the thermal and chemical characteristics of the lower atmosphere are influenced by the ambient concentrations of ozone.

During the past two decades, there has been an increasing realization that man may be inadvertently altering the naturally occurring concentrations of ozone. Namely, supersonic aircraft and industrial chlorofluorocarbon uses may be depleting stratospheric ozone,[1] and other man-made emissions may be increasing tropospheric ozone.[2] Current atmospheric models predict that, should such perturbations continue unabated, the resulting ozone changes could significantly alter surface ultraviolet radiation levels[3] and global climate conditions,[4] thereby adversely affecting human health and society. As a consequence, the importance of detecting temporal and spatial changes in ozone due to man-made causes has been clearly recognized.

Ozone monitoring in one form or another has been underway for many decades. A variety of different approaches and types of instruments have been employed.[5] The total vertical column of ozone has been monitored by ground-based spectrophotometers and satellites. The height profile of ozone has been measured *in situ* by balloon- and rocket-borne instruments and estimated from certain ground-based total-column data. Also some satellite observations can provide low-resolution height-profile data.

While total-column measurements are an indispensable constraint on the abundance of atmospheric ozone and constitute the longest running monitoring record, the *early* detection of ozone changes due to man-made causes has focused on seeking trends in height-profile data. Some man-made perturbations are predicted to cause an ozone depletion in one altitude region and a simultaneous ozone increase in another altitude region, thereby making the total-column change a less sensitive indication of ozone alteration than the height profile.

Over a decade of ozone height-profile data are currently available. However, it is generally agreed that the data are insufficient to detect the decrease in stratospheric ozone that is predicted to have occurred due to man's activities over the last decade. For example, this insufficiency was recently underscored by the National Research Council: "...it is vitally

 0034-6748/83/121719-10$01.30

important to improve and enhance systems for monitoring ozone profiles in the upper stratosphere that could provide a valuable early indication of systematic changes in ozone due to emissions of CFCs (chlorofluorocarbons) or N_2O, but existing data in the upper stratosphere are inadequate for this purpose."[6] This is due to inadequacies in the frequency, geographical distribution, and quality of the data.

Satellite techniques have the potential of furnishing nearly continuous and globally distributed ozone height profiles. However, long-term instrumental drifts have introduced some ambiguities in the deduced trends. Furthermore, since the lower altitude limit for statellite data is about 20 or 25 km, monitoring by satellites of lower-stratospheric and tropospheric ozone, where an increase is predicted, is precluded.

Balloon-borne instruments have provided a substantial body of ozone height profiles in the lower atmosphere, although relatively limited in frequency and global coverage. Furthermore, it has been proposed that such instruments be used for long-term calibrations of satellite sensors. However, the accuracy of balloon-borne instruments is most uncertain in the altitude region where the need for intercomparison is most critical. Namely, the ozone depletion due to chlorofluorocarbon usage is expected to be most sensitively detected above 35 km. At these low pressures, ozone losses inside the instrument and other problems can cause substantial inaccuracy in the data.

Most balloon-borne ozone measurements have been made with instruments that use electrochemical methods.[7–9] The advantage of these techniques is that the instruments are relatively lightweight and inexpensive. Hence, they have served as the mainstay of multistation monitoring networks that employ small balloons and disposable instruments. The effectiveness of the electrochemcial methods declines above about 25 km. The efficiency of the pump, which must be calibrated preflight in the laboratory, deteriorates markedly at the higher altitudes.[10] Also, corrections for background current are not fully characterized, especially at high altitudes.[11] The electrochemical detector has a time response of about a minute.

Chemiluminescent methods[12,13] have been used to obtain ozone profiles in conjunction with multicomponent large-balloon research payloads. This more complex and somewhat heavier sensor affords a rapid time response, a second or less, which is a distinct advantage for investigating chemical and transport phenomena in concert with fast-response detectors for other molecular species. However, the chemiluminescent technique is dependent on laboratory calibrations, which could change in flight. Furthermore, like the electrochemical sensor, its effluent can potentially cause artifacts in other types of sensors on the same payload.

The UV-absorption method[14–18] has one distinct advantage over other techniques; namely, it makes an absolute measurement. The ozone concentration is determined by measuring the amount of 254-nm light that is absorbed by an air sample that flows through an absorption cell. Since the ozone cross section at this wavelength has been accurately measured in the laboratory, the need for any calibration (e.g., pump flow rate) is avoided. A further advantage is that UV absorption is practically nonpolluting and, therefore, can be used alongside other instruments making *in situ* measurements.

The UV-absorption instruments that have been flown by others have all used a single-tube photometer, usually a modified version of a commercial Dasibi laboratory ozone photometer[14] (typically model 1003 AH, Dasibi Environmental Corporation, Glendale, CA),[19] which employs a single, U-shaped, 71-cm-long absorption chamber. The single photometers have all used the Dasibi "count-up/countdown" method for determining the ozone concentration, which requires a complete cycle of the instrument through a reference and a measure mode in order to make a single ozone measurement. During the 10 to 30 s used for this cycling, changes in lamp intensity are accounted for, but not changes in photometer transmission. While the modified Dasibi data are likely to be some of the most accurate ozone height profiles extant, the UV-absorption method can still be improved. Our goal has been to do this.

We have developed a balloon-borne UV-absorption ozone instrument that incorporates several unique improvements over the single-photometer design. As with the independently developed NBS standard ozone photometer,[20] and the commercially available U.V. Photometric O_3 Analyzer, Model 49 (Thermo Electron Corporation, Hopkinton, MD), two absorption chambers are used. These chambers alternate between measure and reference modes, thereby allowing continuous ozone measurements while compensating for both the lamp intensity fluctuations and the photometer transmission changes. The design and construction of the detector and associated electronics yield a sensitivity that permits using a short (40-cm) absorption cell, which reduces weight, temperature gradients, mechanical stresses, and flow time. Furthermore, with short *straight* absorption tubes, chamber surface area and the possibility of turbulence are lessened, thereby reducing the magnitude of potential loss of ozone to the walls, which we believe to be the largest contributor to the measurement uncertainty at altitudes above 35 km.

Measurements can be made in 1 s (8 to 30 times faster than other UV photometers) with a detection limit that is substantially less than the ozone levels encountered at balloon altitudes. This rapid response time makes the instrument suitable for determining detailed vertical ozone profiles not only on balloon ascent, but also on parachute descent, which is particularly valuable in atmospheric chemistry and transport studies. The absolute accuracy of this instrument makes it suitable for determining long-term trends, as well as satellite sensor calibration.

We describe here the design, construction, and laboratory testing of the instrument. Flight performance data that characterize the precision and response time are presented. The overall accuracy obtained in past flights is estimated. Last we discuss the future potential of an extension of the method, namely *three* absorption cells, for an in-flight determination of wall losses. This could provide a highly accurate method of measuring stratospheric ozone at 35 to 40 km, where the need for reliable and accurate ozone measurements is most acute.

I. DESCRIPTION OF INSTRUMENT

The ozone detector described here and shown schematically in Fig. 1 has three basic parts: a UV lamp with its associated optics, two sample chambers (absorption cells) with their flow components, and the detectors. The lamp emits 254-nm radiation that is directed down the length of the sample chambers to the detectors. Since ozone readily absorbs radiation at this wavelength, changes in ozone concentration in either of the chambers will produce a change in intensity at its detector. By using an ozone scrubber, an ozone-free air sample is directed into one chamber, while unaltered air is directed into the other. A four-port valve alternates the scrubbed air between the two chambers. From the measured intensities at the two detectors, the concentration of ozone in the instrument can be calculated.

The sample chambers are 40-cm long and constructed from 2.54-cm-o.d., 1.27-cm-i.d. Teflon (TFE) tubing (Fluorocarbon, Anaheim, CA). These tubes fit inside 1-in. copper tubing and are attached to an aluminum support, onto which mount two pressure-sealed housings, one to contain the lamp and the other to contain the detector electronics. The sample chambers are separated from the pressurized housings by quartz windows on the lamp end and narrow-band filters (20% transmission at 254 nm, 11-nm full-width at half-maximum, Barr Associates, Westford, MA) on the other. These filters eliminate virtually all light that might leak into the chambers and the weak mercury lines near 254 nm (which would otherwise introduce about a 0.5% correction).[21] Silicon O rings are used for the pressure seals. The sample gases pass into the chambers via threaded Teflon (TFE) connectors (LF series, Fluorocarbon, Anaheim, CA) near their ends, and ports for measuring pressure inside the chambers are located at their midpoints. A control unit of our own design regulates the chamber temperature.

Inside the lamp housing are four units: a low-pressure mercury lamp, the lamp power supply, a lamp temperature controller, and a beam-splitter/mirror arrangement. The mercury lamp (L937-03, Hamamatsu Corporation, San Jose, CA) has a Vycor shield to block the radiation that produces ozone, without appreciably attenuating the dominant 254-nm mercury line used for the measurement. The lamp is powered by an 11-kHz 200-V square-wave power supply (420-209, Research Support Institute, Incorporated, Cockeysville, MD). Another control unit senses and regulates the temperature near the lamp. The UV beam splitter (201010, Esco, Oak Ridge, NJ) and UV-enhanced mirror (02MPQ 001/028, Melles Griot, Irvine, CA) are aligned so that the lamp will illuminate the detectors at the opposite end of the sample chambers.

The detector consists of a pair of UV-sensitive photodiodes and their associated circuitry. Since the sensitivity and stability of these detection units are crucial to the performance of the instrument, we show our circuit in some detail in Fig. 2. The UV-enhanced silicon photodiode (1336 BQ, Hamamatsu Corporation, San Jose, CA) is followed by a low-noise operational amplifier (52K, Analog Devices, Norwood, MA) and a 1-MHz voltage-to-frequency (V/F) converter (460L, Analog Devices, Norwood, MA). The solder connections between the detector and amplifier input are carefully isolated from thermal changes, since they can act as thermocouples and, thereby, can introduce spurious signals. The light striking a photodiode produces a current I at the input of the operational amplifier that is proportional to the light intensity. For the three resistor values shown in the feedback circuit, the amplifier's output voltage V is

$$V=\frac{R+1000}{1000}\times 10^{7}\times I. \tag{1}$$

The value for R (typically 10 KΩ) is chosen to produce 8 to 10 V at the input of the V/F converter. All three resistors have a temperature coefficient of 10 ppm/°C or better. The

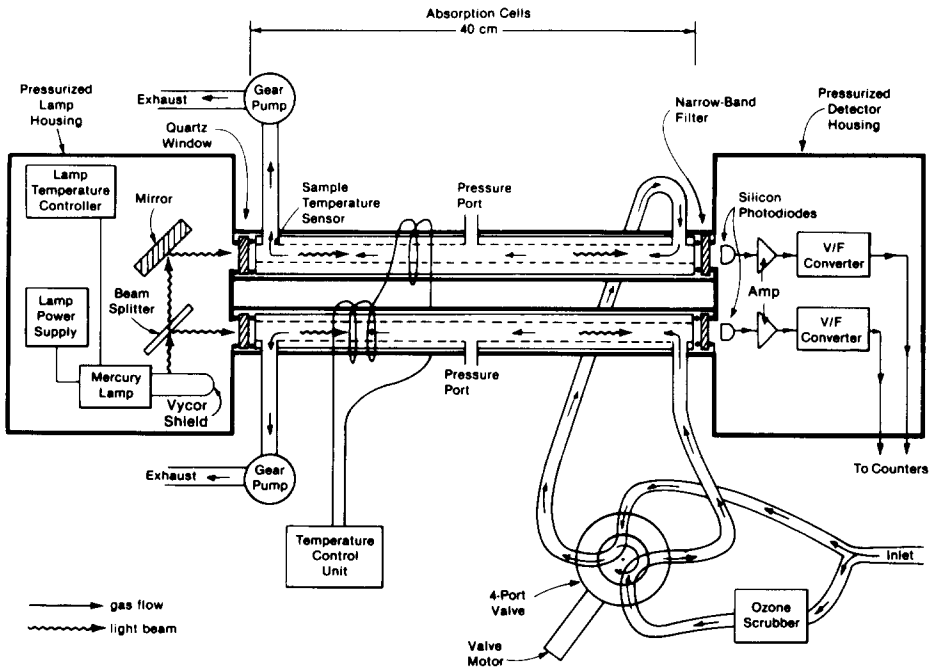

FIG. 1. Schematic diagram of the dual-beam UV-absorption ozone photometer.

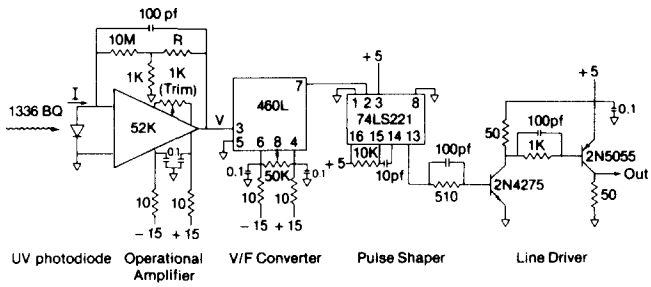

FIG. 2. Circuit diagram of the UV photodiode detector module. The units are ohms, microfarads, and volts, except where noted.

10-MΩ resistor is a thin-film device with a 5-ppm/°C temperature coefficient (TK 633, Caddock Electronics, Inc., Riverside, CA), while the other resistors are wirebound with 10 ppm/°C (7005, RCL Electronics, Manchester, NH). With 10 V at the input of the voltage-to-frequency converter, a 1-MHz square-wave signal appears at its output. The width of these pulses is shortened to 100 ns by the pulse shaper in order to minimize power consumption in the 50-Ω compatible line driver amplifier. The two detector units are electrically shielded from one another to reduce interference, but are thermally connected to reduce thermal gradients in this very sensitive circuit. With a constant current source of about 100 nA at the amplifier input, the output frequency measured each second was stable to $\pm$ 2 ppm over a period of 10 s. The nonlinearity of the detector circuit is determined by that of the V/F converter, which is $\pm$ 0.015% of full scale over its entire range. Since the zero offset of the operational amplifier can be trimmed to zero with the lamp off, the frequency at the output of the detector unit is proportional to the incident light intensity to within a negligible error.

Because this instrument measures changes in transmission through the sample chambers as small as 0.001%, the mechanical and thermal engineering of the chambers and the associated optical components are as important as those of the detector electronics discussed above. Thermal gradients and mechanical stress between the two chambers are decreased by mounting the sample chambers and the pressurized housings to an aluminum support. Heating is done uniformly along the entire length of the chambers and controlled at 35 °C. The lamp temperature is sensed on an aluminum block that surrounds the lamp and is regulated at 40 °C. This helps to minimize lamp intensity fluctuations. The gear pumps are mechanically isolated from the instrument to avoid vibrations. For balloon flights, the instrument is wrapped with aluminum foil and inserted into a 5-cm-thick ethafoam box. This insulation keeps the temperature of the instrument from changing more than a few degrees during the flight.

There are two flow paths through the instrument. The air sample enters a Teflon (TFE) tee, and then, depending on which of the two paths is being followed, either goes directly through Teflon (FEP) tubing (Galtek Corporation, Chaska, MN) to a four-port Teflon (TFE) valve of our own design or enters an ozone scrubber (part No. A-0235, Dasibi Environmental Corporation, Glendale, CA) before going to another port of the valve. This valve is rotated 90° at regular intervals (typically 10 s), thereby alternating the two input flow paths between the two chambers. This has the effect of switching the ozone-free sample (reference gas) between the two chambers. Two gear pumps of our own design are used to pull the samples through the instrument. These pumps are set for a constant pumping speed of about 3 liters/min, which is sufficient for a sample flush time of about 1 s. It should be noted that the sample, except when it goes through the ozone scrubber, passes only through Teflon prior to emerging from a sample chamber. We have found that this minimizes ozone losses in the instrument.

Power is supplied by 14 3-A·h lithium cells ($\pm$ 19.6 V) and 6 30-A·h lithium cells (+ 16.8 V), which will operate the instrument for about 15 h. The total weight of our flight instrument with batteries is 14 kg. The package size of the instrument, including insulation is $83 \times 30 \times 26$ cm, plus the piggy-back container $38 \times 26 \times 19$ cm for the gear pumps, the battery pack, and miscellaneous electrical components. Since this instrument was designed to accompany other instruments in flight, we have not developed it as a stand-alone package, but have used a common flight computer for instrument sequencing, data storage, temperature and pressure measurement, and telemetry. However, this package size would likely accommodate the added components necessary for stand-alone flights, with a total weight of less than 25 kg.

II. FLIGHT PREPARATION

Prior to a balloon flight, the performance of the instrument is bench tested by checking the sample chambers for contamination, the detector outputs for lamp intensity and stability, and the temperatures for proper regulation. If we find the instrument needs to be cleaned, the Teflon parts are washed in a sonic cleaner and rinsed with distilled water. The parts are allowed to dry and then reassembled. Calibration of the pressure sensors is also routinely checked. The instrument is turned on for warmup at least 30 min before launch. We use a baroswitch to turn on the instrument's pumps about 100 s after launch, thereby avoiding ground level contaminants. The inlet is also kept covered until a few minutes before launch.

III. BASIC MEASUREMENTS AND INSTRUMENT SEQUENCING

The fundamental quantities measured from the two sample chambers, denoted here as A and B, are the detector-circuit output pulse frequencies, which are proportional to the UV light intensity at the detector end of the absorption cell. These pulses are counted over a 1-s interval and the sums denoted here as F_A and F_B. As described below, F_A and F_B are sufficient to determine the ozone concentration in the sample chamber. F_A and F_B are determined for 1-s intervals for a period of 10 s, then the four-port valve is rotated by 90°, thereby interchanging the sample and reference modes of the chambers. F_A and F_B are again determined for 1-s intervals for a period of 10 s, followed by another mode interchange. This sequence is continued as long as the data are being acquired.

Figure 3(a) shows an example. The data are from a 1-min slice of the measurements made while at float at 30 km near Palestine, Texas on the afternoon of July 8, 1982. Each filled circle is a raw datum, F_A or F_B, representing the 1-s sum of output pulses and is plotted at time T denoting the end of that 1-s counting period.

Our balloon-flight computer sets the mode interchange rate at 10 s and controls the on-board data storage and sequencing of all of the measurements. These data are also transmitted to our ground station and recorded as a backup. The raw data are later analyzed on a computer using a method described in the following section.

At $T = t - 1$, a valve change occurred that ends chamber A's sample mode and chamber B's reference mode. The first pair of measurements, F_A and F_B, at $T = t$ are affected by the flush time, but it is clear from the second pair of measurements at $T = t + 1$ that this time has been kept sufficiently short to ensure that only one datum has been "spoiled" by the mode switching.

The sample chamber temperature and pressure T_S and P_S and the outside atmospheric temperature and pressure, T_O, and P_O, are required to deduce the desired atmospheric ozone concentrations from those measured inside the absorption chambers. We have found that temperature and pressure differences between the two chambers are negligible and, hence, T_S and P_S are determined from only one chamber. T_S is measured by a curve-matched thermistor (UUA 32J3, Fenwal Electronics, Framingham, MA). P_S has been determined using a variety of transducers, depending on the makeup of the entire payload. Our pressure transducers have been either Digiquartz (model 215-A, Paroscientific Incorporated, Redmond, WA) or Baratron (various models, MKS Instruments Incorporated, Burlington, MA). Typically, P_S and T_S have been measured every 2 and 8 s, respectively.

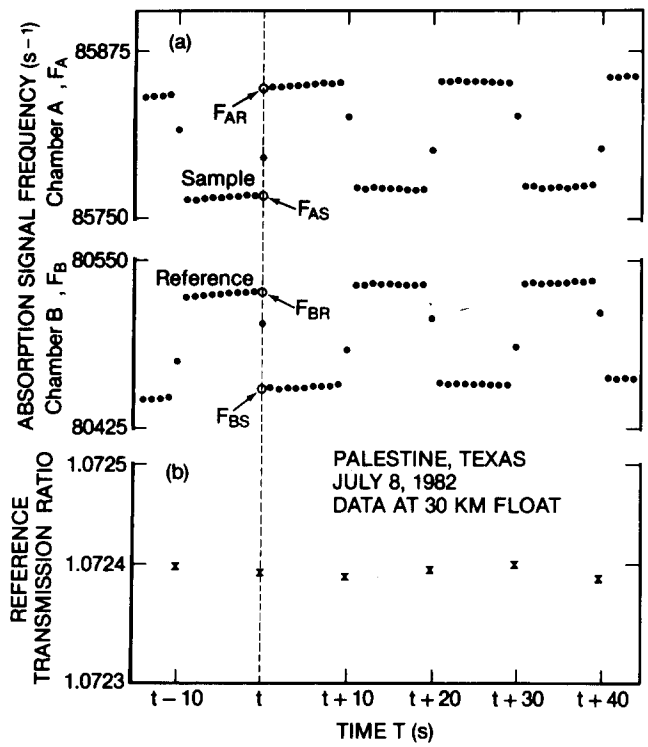

FIG. 3. A 1-min sample of the photometer data taken while the balloon floated at 30 km. Six valve changes are shown. For part (a), each filled circle is a 1-s measurement of the absorption signal frequency for one of the chambers. The open circles are extrapolations of the F_A and F_B data to the mode interchange time t. For part (b), the x's are the reference transmission ratios, REF(T), determined at the mode interchanges via Eq. (10). REF(T) is the transmission of chamber B relative to that of chamber A.

IV. DATA REDUCTION

The relationship beween the quantities measured by this instrument and the concentration of ozone in the sample chamber is derived from the Beer–Lambert expression for a single-chamber photometer

$$\ln(I/I_0) = -L\sigma C_S , \tag{2}$$

where I is the lamp intensity at the detector when the chamber contains the sample gas, I_0 is the same measurement except with the ozone removed, L is the length of the sample chamber, σ is the molecular absorption cross section of ozone at 254 nm, and C_S is the average concentration of ozone in the sample chamber when I was measured. Since L and σ are known quantities, a determination of the transmittance R of the sample chamber from the observed absorption signal frequencies F,

$$R \equiv I/I_0 = F(\text{sample})/F(\text{reference}), \tag{3}$$

yields C_S

$$C_S = -\ln(R)/L\sigma . \tag{4}$$

It is, of course, implicitly assumed in Eq. (4) that the change in F from sample to reference can be attributed solely to the ambient ozone. In practice, instrumental changes can occur over the period during which the sample and reference measurements are made; hence, C_S can be in error. For example, the lamp intensity can drift between sample and reference measurements. Other effects, which we label here as photometer transmission changes (i.e., not ozone and not lamp related), are caused by mechanical or thermal stresses and nonozone absorption. In a preceding section, it was described how the instrument was designed to reduce the effects of lamp and transmission changes. Here we describe how the data reduction methods can also be used to eliminate or further reduce these effects. The discussion focuses on the best way to calculate the transmittance R from the measured F(sample) and F(reference).

The simplest method to obtain R is to treat the instrument as two independent photometers, A and B, and calculate the transmittance of each chamber separately; i.e., a ratio of measurements from the same photometer, but made at different times, as in Eq. (3). For a given chamber, a valve change affords the opportunity to have the sample and reference measurements as close together in time as possible. In Fig. 3, a valve change occurs at $T = t - 1$ and the instrument has settled by $T = t + 1$. Therefore, the transmittance of chambers A and B at the median time $T = t$ are

$$R_A(t) \cong F_A(t-1)/F_A(t+1) \tag{5}$$

and

$$R_B(t) \cong F_B(t+1)/F_B(t-1) . \tag{6}$$

An average 2-s transmittance could be defined by

$$\bar{R}(t) = (R_A + R_B)/2 . \tag{7}$$

However, this method has some clear disadvantages. The sample and reference measurements for each chamber are separated by two seconds and the lamp intensity and chamber transmission may not be constant over that interval. Furthermore, rapid valve changes would be required in order to avoid long intervals between measurements.

A second method avoids one of these disadvantages, namely the effects of lamp intensity changes, by exploiting the fact that *both* chambers are illuminated simultaneously by the same lamp. Here, in contrast to the above method, the key quantity is a ratio of measurements from *different* photometers, but made at the *same* time

$$r(T) \equiv F_A(T)/F_B(T) . \tag{8}$$

Instead of the sum of ratios in Eq. (7), the mean transmittance over a 2-s interval about a valve change is given by the product of ratios:

$$\bar{R}(t) = \left(\frac{F_A(t-1)}{F_B(t-1)}\,\frac{F_B(t+1)}{F_A(t+1)}\right)^{1/2} , \tag{9a}$$

$$\bar{R}(T) = [r(t-1)/r(t+1)]^{1/2} . \tag{9b}$$

Should a lamp intensity change occur between $T = t - 1$ and $T = t + 1$, $F_A(t+1)$ and $F_B(t+1)$ will have been changed by the same factor. Because they appear in Eq. (9a) as a ratio, the effect will cancel. Chamber transmission changes that occur during the course of the measurement can still introduce uncertainties and the applicability of the method is still limited to valve changes. However, the use of ratios of simultaneous signals from the two chambers is a significant advantage, since lamp changes are a major part of potential instrumental shifts. We use this method when we have a counter with a ratio mode available for tests, e.g., in the lab and in the field during flight preparation.

The third and best method of data reduction exploits the two-chamber/signal-ratio approach and recognizes that the relative transmission of the two chambers generally varies slowly compared to the time scale of the valve changes. Hence, it is useful to define the *reference transmission ratio* at a time T, REF(T), as the ratio of chamber B intensity to chamber A intensity that would occur *if* the two chambers were to contain the same gases at time T. We can approximate its values during the flight from the set of data points determined at the valve changes. For example, for the valve change at t pictured in Fig. 3,

$$\mathrm{REF}(t) = \left(\frac{F_{BR}}{F_{AR}}\,\frac{F_{BS}}{F_{AS}}\right)^{1/2} , \tag{10}$$

where F_{AR}, F_{AS}, F_{BR}, and F_{BS} are the extrapolations of the F_A and F_B data to the mode interchange time t. Note that REF(t) is a number that is independent of lamp intensity fluctuations. This can be seen by rearranging the terms in Eq. (10) and noting that extrapolations can be made from ratio measurements of the frequencies F_A and F_B to obtain REF(t), thereby canceling all lamp intensity fluctuations. Since REF(t) is also independent of C_S, it can be considered to be a ratio of transmissions of the two photometers. If both photometers were identical optically, electronically, and mechanically, then REF(t) would equal exactly one and would not change with time. However, this is not the case, so it must be calculated at each mode interchange to update the temporal changes in transmission of the photometers. Figure 3(b) shows a REF(T) variation of a few parts per million during the 30-km float.

Since the relative photometer transmission changes are generally tracked very well by the 10-s mode interchange rate, a linear interpolation between REF($t - 10$) and REF(t) can be used for REF($t - 1$). So if $F_{A0}(t-1)$ is the value for F_A at $t - 1$ if photometer A had been scrubbed of ozone, then

$$\frac{F_B(t-1)}{F_{A0}(t-1)} = \mathrm{REF}(t-1) . \tag{11}$$

Therefore, the transmittance of photometer A at time $T = t - 1$ is

$$R_A(t-1) = \mathrm{REF}(t-1)\,\frac{F_A(t-1)}{F_B(t-1)} , \tag{12a}$$

$$R_A(t-1) = \mathrm{REF}(t-1)\; r(t-1) . \tag{12b}$$

Similarly, since for any time T a value for REF(T) can be obtained by a linear interpolation,

$$R_A(T) = \mathrm{REF}(T)\; r(T) , \tag{13}$$

whenever photometer A is in sample mode. In a similar fashion it can be shown that when photometer B is in sample mode at time T,

$$R_B(T) = \frac{1}{\mathrm{REF}(T)\, r(T)} . \tag{14}$$

This method fully utilizes the dual-beam design of the instrument, yielding continuous 1-s measurements, with only a 1-s interruption in data at each valve change. It is the method that we use to do the final reduction of all of the ozone flight data, which are stored on tape and, hence, the required reference transmission ratios, extrapolations, and interpolations can be done on a laboratory computer.

Once C_S is calculated and we assume negligible ozone losses in the instrument, the concentration of ozone entering the sampling port, [O_3], can be calculated

$$[O_3] = \frac{T_S P_o}{T_o P_S}\, C_S . \tag{15}$$

V. INSTRUMENT PERFORMANCE

Our ozone instrument has been flown six times, attaining altitudes up to 33 km. Its first flight (May 1981) was with our Laboratory's water-vapor instrument.[22] Later flights have been with our nitric-oxide and nitrogen-dioxide instrument.[23] A sample of the ozone height profiles obtained is shown in Fig. 4. These are the "upleg" ozone data obtained on a flight launched at 7:55 CST on August 10, 1982, from Gimli, Manitoba, Canada. The solid line depicted has been drawn from point to point through the approximately 6500 1-s measurements made on the 2-h ascent to reach float. Considerable ozone structure is revealed. In addition to providing ozone data to use in these stratospheric photochemis-

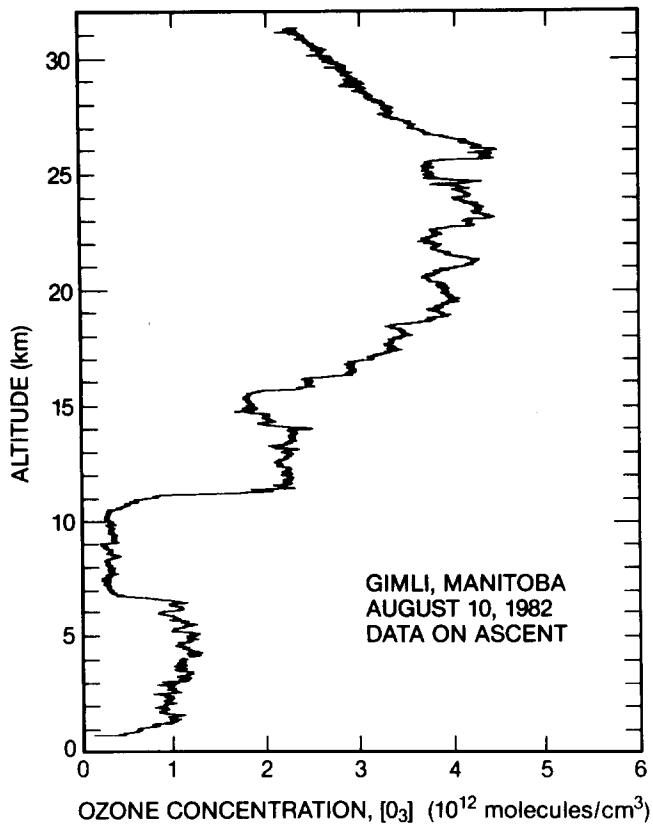

FIG. 4. Ozone height profile on a 2-h ascent taken at a 1-s data rate. The solid line depicted has been drawn from point to point through the approximately 6500 measurements.

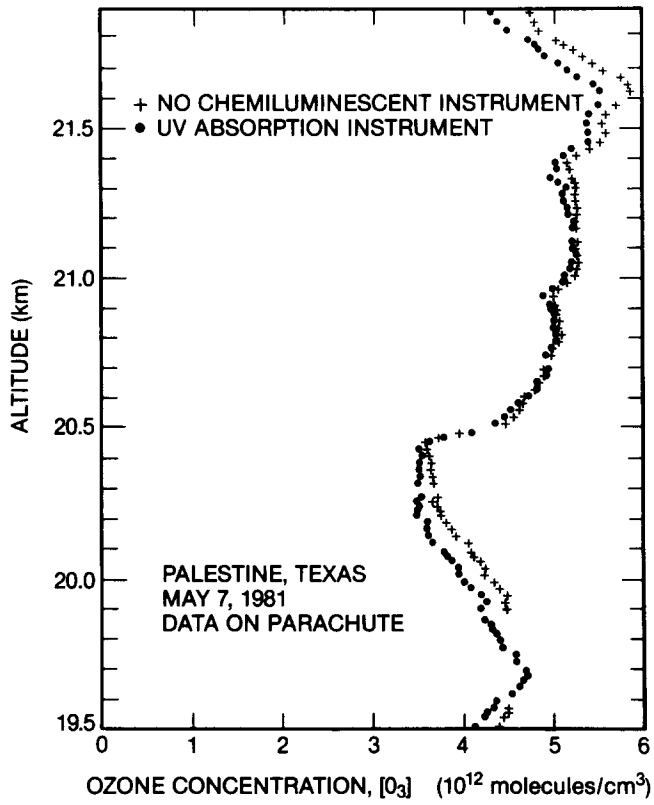

FIG. 5. Ozone measurements made by two ozone instruments while on the same gondola. The filled circles represent 1-s measurements made by the present UV-absorption photometer. The pluses denote 1-s measurements made by our Laboratory's chemiluminescent instrument.[24] Note expanded vertical scale of the figure.

try and dynamics experiments, these profile data also demonstrate the ozone instrument's performance characteristics. We report these diagnostic aspects of some flight results here, along with the test data from laboratory investigations.

A. Response time

The structure in the ozone profile in Fig. 4 gives a good indication of the instrument's very rapid response time. For example, the extremely sharp increase in ozone at 11 km (more than a 200% increase within 90 m) is defined by 20 1-s measurements. All of the major variations shown are atmospheric ozone changes, not noise. This assertion is supported by the data in Fig. 5. On this May 7, 1981 flight from Palestine, Texas, the UV-absorption instrument was accompanied by our Laboratory's nitric-oxide chemiluminescent ozone instrument.[24] The portion of data shown on the expanded vertical scale in Fig. 5 was taken by the two instruments while on parachute descent between 22 and 19.5 km. Each datum represents a 1-s measurement. At 20.5 km, there is a 20% change in ozone within 60 m and in a 5-s time interval. Both instruments, which have response times of 1 s or less, track the ozone variations in concert.

B. Precision

The precision of the instrument has been assessed in three different ways. First, laboratory measurements are used to determine the minimum detectable concentration. Second, flight measurements made during a 30-km float are similarly analyzed. Last, the contribution to the precision due to changes in the reference transmission ratio, REF(T), during flight are evaluated. It should be noted that small changes in light intensity are being measured (always less than 0.5% in the atmosphere), so the precision is not dependent upon the concentration of ozone.

For the laboratory measurements, the ozone measured by our instrument was generated by a Dasibi model 1008AH. The standard deviations about the mean of the 1-s measurements over a 100-s time interval were calculated for a wide range of ozone concentrations. The resulting standard deviations increased from 1.5×10^{10} molecules/cm^3 at undetectable levels of ozone to 3×10^{10} at 8×10^{12} molecules/cm^3, the latter being a higher concentration than that encountered in the stratosphere. We believe that the value of 1.5×10^{10} is a measure of the inherent noise of the instrument, since the larger standard deviations appeared to be due to short-term fluctuations in the ozone source operating at the higher concentrations.

A similar analysis was made during a 30-km balloon float, where the ambient ozone concentration was 3.1×10^{12} molecules/cm^3. Figure 3 shows a 1-min interval of these data. A standard deviation of 2.1×10^{10} was obtained, only slightly larger than the laboratory value. Although more variation would be expected on a flight than in the lab, it is

possible that some of the observed variation is due to ozone losses to the balloon or its payload.

The final method was to consider the changes in REF(T) during a flight to quantitatively assess the assumption that changes in transmission of the two photometers is slow compared to the rate at which REF(T) is being measured. Changes in REF(T) can be due to contamination in the photometer and mechanical stresses, which alter the optical paths. Vibration and acceleration cause these mechanical stresses, in addition to rapid changes in temperature and pressure. By considering two reference transmission ratios at adjacent valve changes, an artifact concentration can be calculated

$$\Delta C_S = \ln(\mathrm{REF}(T1)/\mathrm{REF}(T2))/L\sigma\,. \quad (16)$$

This artifact is the difference between the two values computed for C_S using REF($T1$) and REF($T2$) for the calculations. Typical values for ΔC_S during the 30-km float just discussed above are 2×10^{10} molecules/cm^3, that is, the REF(T) updates that are made every 10 s affect the value of the ozone concentration calculated by an amount comparable to the laboratory standard deviation. Since the values used for REF(T) in calculating C_S are interpolations between successive valve changes, the contribution from REF(T) to the standard deviations calculated is less than, or at worst, comparable to the standard deviation in the observed ozone concentration.

During ascent and parachute descent, we see larger changes in REF(T), implying larger standard deviations, which arise from the severe mechanical stresses and other causes. The worst conditions occur shortly after the time when the parachute opens, when we commonly see one to four large abrupt changes in REF(T). For each abrupt change, we must ignore 1 to 10 s of data. Otherwise, typical values for ΔC_S on the remainder of the descent are 1×10^{11} molecules/cm^3. Moreover, we observe smooth, nonrandom changes in REF(T), thereby fulfilling our assumption that the changes in transmissions of the two photometers is adequately tracked by the reference measurements made every 10 s. Therefore, on parachute descent, the linear interpolations made between successive reference transmission ratios are quite important and clearly improve the final data. With these improvements, a precision of about 3×10^{10} molecules/cm^3 during parachute descent seems appropriate.

Part (a) of Table I summarizes the one-standard-deviation precisions that characterize the 1-s measurements of the instrument. To put these in an atmospheric context, the minimum detection limit is 0.3% of the typical ozone maximum of 5×10^{12} molecules/cm^3 at 22 km and 2.5% of the typical concentration of 6×10^{11} molecules/cm^3 at 8 and 40 km. Of course, measurement periods longer than 1 s can be used to improve the precision further when the ambient ozone being sampled is expected to be relatively constant, e.g., at float.

TABLE I. Observed and estimated uncertainties of the UV-absorption ozone instrument.

(a) Observed precision (one standard deviation) of a 1-s measurement under different lab and flight conditions:

location	precision (molecules/cm^3)
minimum detection limit (lab)	1.5×10^{10}
balloon ascent, float, or valved descent	2.0×10^{10}
parachute descent	3.0×10^{10}

(b) Estimated accuracy:

contributor		estimated contribution (%)
σ and L		2
P and T		<1
wall loss		(i) ~0 at 22 km, ozone maximum
		(ii) $\lesssim2$ below 30 km,
	Net:	(iii) unknown above 30 km

Absolute accuracy: $\lesssim3\%$ plus wall losses, believed to be $\lesssim2\%$ below 30 km

Relative (to σ) acccurcy: $\lesssim1\%$ plus wall losses, believed to be $\lesssim2\%$ below 30 km

(c) Overall maximum uncertainty (one standard deviation, 1-s precision plus accuracy):

location (km)	uncertainty (%)
30	0.8 (on balloon) + 3% (plus wall losses, believed to be $\lesssim2\%$ below 30 km)
22 (ozone maximum)	0.6 (on chute) + 3% (wall losses believed to be negligible)

C. Accuracy

The primary contributors to the absolute accuracy of C_S are the uncertainty in the path length L; the uncertainty in the molecular absorption cross section of ozone σ; and the ozone losses within the instrument. The path length is known to better than $\pm0.2\%$, including estimates for multiple reflections within the chambers.

The uncertainty in σ is generally considered to be $\pm1.5\%$. The currently accepted value[25] for σ at 22 °C is 1.147×10^{-17} molecules/cm^2 (or equivalently 308.32 cm^{-1} atm^{-1} base e absorption coefficient). It is, for example, used by the National Bureau of Standards in Washington in their standard ozone calibrations. The temperature dependence of σ at 254 nm was examined in 1953 by Vigroux,[26] who found a 2% increase in σ by decreasing the temperature from 18° to − 30° C. Bass[20] has been reexamining this temperature dependence and his preliminary results indicate approximately a 1% increase in σ by decreasing the temperature from 27° to − 73° C. No measurements for pressure dependence of σ are available, but pressure is generally considered to have no appreciable effect.[25] However, it is conceivable that for 10° C changes and pressures down to 2 Torr (corresponding to 40 km), the cross section could change by a few tenths of a percent. We approximate the combined uncertainties in L and σ with a value of $\pm2\%$.

Ozone losses within the instrument are likely to be the primary contributor to inaccuracies at 35 km and above. These losses are generally considered to occur on wall surfaces, rather than from any gas-phase photochemical de-

struction within the sample chambers, since the dominant photochemical processes that destroy ozone have time constants much longer than the 1-s residence time within the chambers.

Laboratory measurements[27] support a theoretical $P^{-2/3}$ dependence of wall loss for trace constituents in laminar flow, where P is the total pressure. These studies also found large increases in wall losses when the flow changes from laminar to turbulent. We have made preliminary laboratory measurements that also resemble the $P^{-2/3}$ dependence, finding about 5% loss at pressures corresponding to 40 km, less than 2% corresponding to 30 km, and less than 1% corresponding to 25 km. Since all of our flights thus far have been only to 33 km or below, we have not pursued the ozone wall-loss problem, but feel confident that these losses in our lab tests were indeed wall losses. We would have to consider them in greater detail when making measurements up to 40 km. A method for measuring wall losses during the flight will be discussed in our concluding remarks.

Since measured pressures and temperatures are required to deduce the ambient atmospheric ozone concentration at the instrument's inlet from the measured chamber concentration [Eq. (15)], additional uncertainties arise. However, by choosing appropriate temperature and pressure sensors, their combined contribution can be kept below 1%.

Another factor that could affect the accuracy of balloon-borne ozone measurements is the potential ozone loss due to the balloon and its payload. Although we do not include this loss here in our analysis of the accuracy of our instrument, the present study has suggested a method whereby the magnitude could be assessed. In a previous section, we compared 30-km float variations in ozone to those in laboratory data. The short-term fluctuations in ozone that were in excess of the inherent noise of the instrument were conjectured to be possibly such balloon or payload losses. These fluctuations were only 6×10^{9}, which are negligible at 30 km. Such measurements at a maximum altitude float give an upper limit on these losses for any particular balloon flight.

The factors that contribute to the accuracy of the present instrument are summarized in part (b) of Table I. Since our experience with potential wall losses is limited to about 30 km or less, we qualify, for now, this accuracy component to that altitude range. As indicated in Table I, we sum the components to obtain a net estimated accuracy of $\lesssim 3\%$, plus wall losses, which we believe to be $\lesssim 2\%$ below 30 km. For monitoring, where repeated measurements are made for studying trends, i.e., balloon-satellite comparisons, the accuracy of the measurement relative to σ is also important and we give this separately.

D. Overall uncertainty

Part (c) of Table I summarizes the overall maximum uncertainties (precision plus accuracy) at two altitudes. In these altitude ranges, the precision is a small part of the overall uncertainty. A typical overall uncertainty is 4%, which we believe to be a maximum because all components were simply summed.

VI. CONCLUDING REMARKS

The UV-absorption ozone instrument that we have described was designed and used for making simultaneous measurements with other molecular species to study atmospheric dynamics and photochemistry. A fast time response and good precision is necessary for detecting the fine vertical structure common in the troposphere and the lower stratosphere, due to the rapid balloon ascent and parachute descent rates. Furthermore, accurate concentrations are necessary for testing multiple-species measurements against model predictions. The instrument has met and often exceeded those design criteria on several balloon flights to altitudes up to 33 km. We have also constructed a modified version, which we have not yet flown. It incorporates four modifications that should yield improved performance. First, we have replaced the support for the sample chambers with a rigid single-piece aluminum construction that completely houses the Teflon tubes. We expect that this will improve the mechanical and thermal stability of the chambers, especially on parachute descent. Second, we have included the photodiodes inside the pressurized detector housing (as we have actually indicated in Fig. 1). This should improve the stability of the reference transmission ratio when going through rapid pressure changes. Third, we incorporated a lamp power suppy of our own design, which laboratory tests had shown to be more stable and which may, therefore, improve the precision. Last, larger-diameter fittings and shorter inlet tubes will reduce the possibility of wall losses at high altitudes.

As discussed in the Introduction, there is a strong need for precise and accurate ozone measurements up to 40 km, where early trend detection and balloon/satellite intercomparisons can be most sensitively done. The present UV-absorption instrument has existing capabilities and future potential that can contribute to that need. Its precision is already adequate. For example, at 40 km, the one-standard-deviation precision expected from a 10-s measurement at float (Table I) would be 1% of the typical ozone concentration at this altitude. The accuracy relative to the ozone absorption cross section would be 1% (Table I) if wall losses could be accounted for. Therefore, if the uncertainty in the magnitude of the wall losses could be reduced to 3%, then the UV-absorption instrument has the potential of making ozone concentration measurements at 40 km with an estimated overall relative uncertainty of $\lesssim 5\%$. Since it has been proposed that wall losses could be as large as 30% at 40 km (Ref. 27), it is clear that the key to achieving an overall relative uncertainty of $\lesssim 5\%$ is a major reduction in the uncertainty in wall losses.

There must be considerable work done on reducing or quantifying wall losses if this overall uncertainty is to be obtained at 40 km or higher. One approach would be to explore laboratory measurements and calibrations, as well as passivation techniques. However, even with careful work, the wall losses could vary considerably from flight to flight and there would be no way to check in the laboratory for in-flight changes. We believe that in-flight measurements of wall losses are not only possible, but also are essential if wall-loss corrections are to be made to the data with confidence.

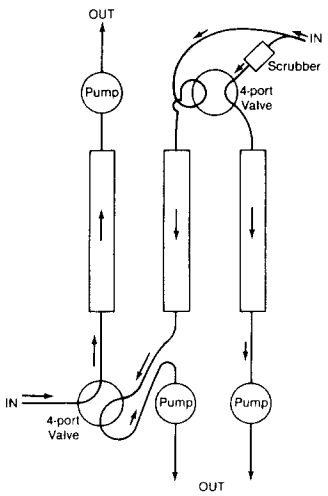

FIG. 6. Schematic diagram of the proposed three-chamber UV-absorption ozone photometer for making inflight wall-loss measurements.

One method for in-flight measurements of wall losses would simply be to fly two UV-absorption ozone instruments side by side with appropriate valving and plumbing to sequentially operate them in series and then in parallel, so that one of the instruments, call it A, is measuring the ozone just measured by the other, call it B. This gives A a calibrated source of ozone to measure. Its measurement would differ from the measurement made in B by the ozone lost in A, thereby measuring the percent wall loss in A. By sequencing A to then sample ambient air, as is B, the measurement of A can be corrected for wall losses. From this, one can also obtain the wall losses in B. Then one has two measurements of ozone, each corrected for wall losses. A key feature of properly designed UV photometers that allow them to be placed in series is that the absorption measurement is virtually nonpolluting.

This principle could be incorporated into a three-chamber photometer, as shown schematically in Fig. 6, which with appropriate valving would also measure in-flight wall losses. Interconnections between the photometers must be carefully laid out to minimize any uncertainties in wall losses introduced by changes in flow paths.

Hence, it is clear that a multitube UV absorption photometer—with its inherent fast time response, good precision, high accuracy, and the potential to measure wall losses *in situ*—holds considerable promise for reliable ozone measurements at 40 km.

ACKNOWLEDGMENTS

We wish to express our appreciation to D. L. Albritton and M. McFarland and to our other colleagues in the Aeronomy Laboratory for their suggestions and encouragement. We also acknowledge the valuable balloon-launch assistance of three groups: Department of Physics and Astronomy at the University of Wyoming, National Scientific Balloon Facility in Palestine, Texas, and National Research Council of Canada Gimli Balloon Facility. We thank J. Waters for her expert preparation of the manuscript. The development of this instrument was supported, in part, by the Federal Aviation Administration.

[1] *The Stratosphere, 1981: Theory and Measurements*, WMO Global Ozone Research and Monitoring Project Report No. 11 (World Meteorological Organization, Case Postale No. 5, Geneva 20, Switzerland, 1982), pp. 3-1–3-28.
[2] S. C. Liu, D. Kley, M. McFarland, J. D. Mahlman, and H. Levy II, J. Geophys. Res. **85**, 7456 (1980); also see references therein.
[3] S. Nachtwey and R. D. Rundel, "Ozone Change: Biological Changes," in *Stratospheric Ozone and Man, Vol. II*, edited by Frank A. Bower and Richard B. Ward (CRC Press, Boca Raton, FL, 1982), Chap. 4.
[4] *Potential Climatic Effects of Ozone and Other Minor Trace Gases*, WMO Global Ozone Research and Monitoring Project Report No. 14 (World Meteorological Organization, Case Postale No. 5, Geneva 20, Switzerland, 1982).
[5] Julius London and James K. Angell, "The Observed Distribution of Ozone and its Variations," in *Stratospheric Ozone and Man, Vol. I*, edited by Frank A. Bower and Richard B. Ward (CRC Press, Boca Raton, FL, 1982), Chap. 1; also see pp. 1-60–1-75 of Ref. 1.
[6] *Causes and Effects of Stratospheric Ozone Reduction: An Update* (National Academy Press, Washington, 1982), pp. 26–27.
[7] A. W. Brewer and J. R. Milford, Proc. R. Soc. London, Ser. A **256**, 470 (1960).
[8] W. D. Komhyr, Ann. Geophys. **25**, 203 (1969).
[9] W. D. Komhyr and T. B. Harris, "Development of an ECC ozonesonde," NOAA Tech. Report No. ERL 200-APCL 18, 54 pp., 1971.
[10] A. L. Torres, "ECC ozonesonde performance at high altitudes: pump efficiency," NASA Tech. Memo. 73290, 1981.
[11] Donald C. Thornton and Nagla Niazy, J. Geophys. Res. **87**, 8943 (1982).
[12] Victor H. Regener, J. Geophys. Res. **69**, 3795 (1964).
[13] Patrick Aimedieu and Jean Barat, Rev. Sci. Instrum. **52**, 432 (1981).
[14] Lloyd D. Bowman and Richard F. Horak, "A Continuous Ultraviolet Absorption Ozone Photometer," in *Air Quality Instrumentation, Vol. 2*, edited by J. W. Scales (Instrument Society of America, Research Triangle Park, NC, 1974).
[15] Ernest Hilsenrath and Thomas E. Ashenfelter, "A balloon ozone measurement utilizing an optical absorption cell and an ejector air sampler," NASA Tech. Note D-8281, 1976.
[16] E. J. Maier, A. C. Aikin, and J. E. Ainsworth, Geophys. Res. Lett. **5**, 37 (1978).
[17] John E. Ainsworth and James R. Hagemeyer, "Measurement of ozone by a DASIBI ozone monitor," in *The Stratcom VIII Effort*, edited by E. I. Reed, NASA Tech. Paper 1640, p. 95, 1980.
[18] Donald E. Robbins, "NASA-JSC ozone observations for validation of Nimbus 7-LIMS data," NASA Tech. Memo. 58227, 1980.
[19] The commercial instruments, parts, or materials are identified in this paper in order to adequately specify the apparatus and procedures. In no case does such identification imply recommendation, endorsement, or that the item is the best available for the purpose.
[20] A. M. Bass (private communications).
[21] J. R. Hagemeyer and J. E. Ainsworth, Rev. Sci. Instrum. **53**, 1090 (1982).
[22] Dieter Kley and Edward J. Stone, Rev. Sci. Instrum. **49**, 691 (1978).
[23] Brian A. Ridley, Mack McFarland, and Michael H. Proffitt, "Stratospheric NO and NO_2 measurements," paper to be presented at American Geophysical Union meeting, Baltimore, MD, June 1983.
[24] Our nitric oxide chemiluminescent ozone instruments were designed and built by John W. Drummond, Boris Siegel, and Mack McFarland.
[25] A. G. Hearn, Proc. Phys. Soc. London **78**, 932 (1961).
[26] Ernest Vigroux, Ann. Phys. (Paris) **8**, 709 (1953).
[27] J. E. Ainsworth, J. R. Hagemeyer, and E. I. Reed, Geophys. Res. Lett. **8**, 1071 (1981).